RSC Advances

ROYAL SOCIETY OF CHEMISTRY

www.rsc.org/advances

Cite this: DOI: 10.1039/c0xx00000x

www.rsc.org/xxxxxx

ARTICLE TYPE

The photocatalysis from a series of polyoxoazocobaltate high-nuclearity nanoclusters

Bao Mu, Qing Wang, Ru-Dan Huang*

Key Laboratory of Cluster Science of Ministry of Education, School of Chemistry, Beijing Institute of Technology, Beijing, 100081, P. R. China

Received (in XXX, XXX) Xth XXXXXXXXX 20XX, Accepted Xth XXXXXXXXX 20XX

DOI: 10.1039/b000000x

Three $\{Co_{20}\}$ nanoclusters possessing photocatalytic activity, namely, $[Co_{20}(OH)_{24}(MMT)_{12}(SO_4)](NO_3)_2\cdot 6H_2O$ (**1**), $[Co_{20}(MT)_{12}(\mu_3\text{-}OH)_{23}(\mu_3\text{-}O)(SO_4)(CH_3O)]\cdot 2EtOH$ (**2**) and $[Co_{20}(AMT)_{11}(MT)(\mu_3\text{-}OH)_{22}(\mu_3\text{-}O)_2(SO_4)(H_2O)]\cdot EtOH\cdot 4H_2O$ (**3**) (MMT = 2-mercapto-5-methyl-1,3,4-thiadiazole, MT = 2-mercapto-1,3,4-thiadiazole, AMT = amino-5-mercapto-1,3,4-thiaoldiaze and EtOH = ethanol) have been obtained under the hydrothermal condition. Compound **1** that has been reported presents a homometallic Co^{II} cluster containing the α-Keggin polyoxometalate structure. Compound **2** features a cobalt cluster including the α-Keggin-type polyoxoazocobaltate $\{Co_{12}\}$ core, capped by seven octahedral Co^{II} ions and one square-pyramidal Co^{II} ion. Different from compounds **1** and **2**, compound **3** possesses the semi-open square-pyramidal-based $\{Co_{10}\}$ core, and ten octahedral Co^{II} ions are distributed around the core cluster. Through the comparison from structures of compound **1** and compounds **2**–**3**, the different substituent groups of the organic ligands play an important role in the formation of the final homometallic Co^{II} clusters. The electrochemical behaviors of the title compounds at room temperature have been investigated. Moreover, the high-nuclearity metal clusters are firstly acted as photocatalysts to be researched, and then the photocatalytic properties show that compounds **1**–**3** as the potential photoactive materials have the selectivity for degradation of some organic dyes.

Introduction

Environmental pollution is a growing problem that people pay close attention to for a long time because it not only influences the daily life of people, but also restricts the economic development.[1] Water pollution is a main factor to environmental pollution, and its major sources contain domestic sewage, agricultural wastewater and industrial wastewater. Organic dyes, as a kind of industrial products, have been widely applied in many industries, such as leather, papermaking and the dyeing of cotton, artificial fiber and silk.[2] However, those organic dyes possessing the chromophore azo group (–N=N–) pollute the water due to the formation of toxic contaminants and generation of numerous new pollutants.[3] As a result, searching the reasonable solutions is the key to degrade the dye effluents. In various methods, photocatalysis can be viewed as a type of ecological technology for the abatement of organic dyes from wastewater.[4] Except that the conventional semiconductor metal oxides, such as TiO_2, gain a wide range of applications.[5] Various new photocatalytic materials based on metal-organic compounds have been devised, which gradually become the focus of research.[6] Metal-organic compounds contain both inorganic and organic moieties, different interaction from which can lead to different charge transfer between metal and organic ligands from the tunable photocatalysts.[7] So far as we know, several metal-organic compounds have been proved to hold excellently photocatalytic effect in respect of degrading organic dye molecules.[8] Designing and preparing the efficient photocatalysts based on metal-organic compounds will be a significant challenge.

Metal-organic compounds include not only the common metal-organic frameworks (MOFs),[9] but also the intriguing metal-organic clusters.[10] Among these, metal-organic clusters of more than 10 metals relative to low-nuclearity clusters are difficult to be obtained. In recent years, some research groups devote themselves to research the construction and performance of the high-nuclearity clusters based on the late transition metals.[11-15] To the best of our knowledge, the reports about the metal-rich clusters (nuclearity ≥10) based on the late transition metals are limited to date.[16] Thus, the synthetic strategy of high-nuclearity clusters with fascinating skeletons and excellent performances needs further research at the present stage.

Key Laboratory of Cluster Science of Ministry of Education, School of Chemistry, Beijing Institute of Technology, Beijing, 100081, P. R. China; Email: huangrd@bit.edu.cn

†Electronic Supplementary Information (ESI) available: IR, TG and additional figures. CCDC: 1418337−1418338. For ESI and crystallographic data in CIF or other electronic format see DOI: 10.1039/b000000x.

According to the recent reports, in the process of building high-nuclearity clusters, various commonly influential factors, such as the reaction time, pH value and so on, can produce an effect on the formation of high-nuclearity clusters with different metal numbers.[17] However, it is rare that the distinctions of the substituent groups from organic ligands influence the construction of different cluster skeletons bearing the same metal nuclear numbers. From this perspective, we chose the late transition metal Co^{II} ions and the other two mercapto-based sulfur aza-heterocyclic ligands with different substituent groups (MT = 2-mercapto-1,3,4-thiadiazole, AMT = 2-amino-5-mercapto-1,3,4-thiadiazole) instead of MMT ligand (2-mercapto-5-methyl-1,3,4-thiadiazole) that we previously used from the reported $[Co_{20}(OH)_{24}(MMT)_{12}(SO_4)](NO_3)_2{\cdot}6H_2O$ (**1**)[15b] to obtain two novel {Co_{20}} nanoclusters, namely, $[Co_{20}(MT)_{12}(\mu_3\text{-}OH)_{23}(\mu_3\text{-}O)(SO_4)(CH_3O)]{\cdot}2EtOH$ (**2**) and $[Co_{20}(AMT)_{11}(MT)(\mu_3\text{-}OH)_{22}(\mu_3\text{-}O)_2(SO_4)(H_2O)]{\cdot}EtOH{\cdot}4H_2O$ (**3**) (EtOH = ethanol). The influence of substituent groups of the ligands on the nanoclusters has been discussed, and the electrochemical behaviors and photocatalytic properties of the title compounds have been investigated. It is noteworthy that the reported high-nuclearity clusters have been researched in the fields of electrochemistry, magnetism, photoluminescent, and so on.[18] However, there is no report about photocatalytic properties of the high-nuclearity nanoclusters based on the late transition metals so far. So in this paper, three {Co_{20}} nanoclusters firstly served as the photoactive candidates are studied.

Experimental

Materials and characterization

All the reaction materials were obtained from commercial suppliers without further purification. Elemental analyses (C, H, N) were carried out on a Perkin-Elmer 2400 CHN elemental analyzer. FT-IR spectra (KBr pellets) were measured on a Nicolet 170SX spectrophotometer. Thermogravimetric (TG) analyses were performed with a Exstar SII TG/DTA 7200 integration thermal analyzer. The powder X-ray diffraction (PXRD) were recorded on a Siemens D5005 diffractometer (Cu Ka radiation, λ = 1.5410 Å). Electrochemical measurements were carried out with a CHI 660E Electrochemical Quartz Crystal Microbalance. In the three-electrode system, the compound bulk-modified carbon paste electrode (CPE), Ag/AgCl and the platinum wire were used as the working electrode, reference electrode and auxiliary electrode, respectively. UV-vis absorption spectra were measured on a TU-1901 UV-vis spectrophotometer.

Synthesis of $[Co_{20}(MT)_{12}(\mu_3\text{-}OH)_{23}(\mu_3\text{-}O)(SO_4)(CH_3O)]{\cdot}2EtOH$ (2).

The mixture of $Co(NO_3)_2{\cdot}6H_2O$ (0.1460 g, 0.50 mmol) and MT (0.0590 g, 0.50 mmol) were dissolved in distilled water (2 mL) and ethanol (2 mL). The triethylamine/ethanolamine of 6:1 (v:v) was added to the reaction solution, and the mixture was sealed into a 25 mL Teflon-lined autoclave, keeping at 110°C for 3 days. When the Teflon-lined autoclave was cooled to room temperature, the red block crystals were obtained. Yield 8% based on Co. Elemental analysis (%) calcd. for $C_{29}H_{50}Co_{20}N_{24}O_{31}S_{25}$: C, 10.85; H, 1.57; N, 10.47%. Found: C, 9.58; H, 1.21; N, 10.81%. IR (KBr pellet, cm^{-1}): 3449(s), 2962(w), 2927(w), 2422(w), 1617(m), 1496(m), 1432(m), 1379(s), 1301(m), 1209(s), 1088(s), 1032(s), 974(m), 893(w), 776(m), 682(w), 615(m), 513(m).

Synthesis of $[Co_{20}(AMT)_{11}(MT)(\mu_3\text{-}OH)_{22}(\mu_3\text{-}O)_2(SO_4)(H_2O)]{\cdot}EtOH{\cdot}4H_2O$ (3).

The synthetic procedure of compound **3** was similar to that of **2** except for using AMT (0.0536 g, 0.40 mmol) instead of MT, and the triethylamine/ethanolamine of 4:1 (v:v) was added to the reaction solution. The red block crystals were isolated. Yield 6% based on Co. Elemental analysis (%) calcd. for $C_{26}H_{61}Co_{20}N_{35}O_{34}S_{25}$: C, 9.22; H, 1.81; N, 14.47%. Found: C, 8.79; H, 1.42; N, 15.03%. IR (KBr pellet, cm^{-1}): 3407(s), 3168(s), 2428(w), 1609(s), 1530(s), 1404(s), 1382(s), 1334(s), 1085(s), 1041(s), 881(w), 832(w), 767(m), 698(w), 615(m), 504(w).

Table 1 Crystal data and structure refinement for compounds **2**-**3**

Compound	**2**	**3**
Empirical formula	$C_{29}H_{50}Co_{20}N_{24}O_{31}S_{25}$	$C_{26}H_{61}Co_{20}N_{35}O_{34}S_{25}$
Formula weight	3211.14	3388.27
Crystal system	Monoclinic	Triclinic
Space group	*P*2(1)/*n*	*P*–1
a (Å)	14.1530(15)	14.5685(13)
b (Å)	26.480(3)	17.4950(19)
c (Å)	32.518(3)	25.288(2)
α (°)	90.00	89.739(2)
β (°)	114.332(2)	79.136(1)
γ (°)	90.00	66.413(1)
V (Å^3)	11104.4(18)	5783.0(10)
Z	4	2
D_c (g cm^{-3})	1.866	1.865
μ (mm^{-1})	3.430	3.300
F (000)	6112	3172
Reflection collected	54344	29440
Unique reflections	19557	20051
parameters	1229	1198
R_{int}	0.1532	0.1365
GOF	1.032	1.063
$R_1{}^a$ [$I > 2\sigma(I)$]	0.1038	0.1009
$wR_2{}^b$ (all data)	0.2455	0.2403

[a] $R_1 = \Sigma||F_o|-|F_c||/\Sigma|F_o|$, [b] $wR_2 = \Sigma[w(F_o^2-F_c^2)^2]/\Sigma[w(F_o^2)^2]^{1/2}$

Preparation of 1–, 2–, and 3–CPEs.

The compound **1** bulk-modified carbon paste electrode (**1**–CPE) was fabricated by grinding the mixture of 0.032 g compound **1** and 0.5 g graphite powder in the agate mortar for about half an hour. 0.18 mL paraffin oil was added into the mixture and stirred with a glass rod. The homogenized mixture was packed into a 3 mm inner diameter glass tube with length of 0.7 cm. The electrical contact was built by the copper rod. The preparation processes of **2**–, **3**–CPEs and the bare CPE without cobalt compounds were similar with that of **1**–CPE.

X-Ray crystallographic study

Single-crystal X-ray diffraction data of compounds **2**–**3** is measured on a Bruker APEX diffractometer with Mo Kα (graphite monochromator, λ=0.71073 Å) at 298 K. The structures were solved through direct methods with SHELXTL crystallographic software package, and they were refined on F^2 through full-matrix least-squares with SHELXL.[19a] All the non-

hydrogen atoms were refined anisotropically. The carbon, nitrogen or sulfur bound hydrogen atom positions were calculated theoretically. The SQUEEZE program of PLATON was used for compounds **2**–**3** because of the existence of disordered solvent molecules.[19b] The crystallographic data of compounds **2**–**3** is summarized in Table 1. Selected bond distances (Å) and angles (°) of compounds **2**–**3** are listed in Table S1 (Supporting Information). CCDC reference numbers are 1418337 for **2** and 1418338 for **3**, which are obtained by the Cambridge Crystallographic Data Center.

Results and Discussion

Description of Crystal Structures

Crystal structure of $[Co_{20}(MT)_{12}(\mu_3\text{-}OH)_{23}(\mu_3\text{-}O)(SO_4)(CH_3O)]\cdot 2EtOH$ (2)

The single-crystal X-ray diffraction shows that compound **2** crystallizes in the monoclinic space group P2(1)/n. Compound **2** is considered as a homometallic {Co_{20}} nanoscale cluster consisting of a α-Keggin polyoxoazocobaltate ion $[Co_{12}(MT)_{12}(\mu_3\text{-}OH)_{23}(\mu_3\text{-}O)(SO_4)]^{15-}$ and eight capped Co^{II} ions (Fig. 1). The generation of $[SO_4]^{2-}$ and $[CH_3O]^-$ may be from decomposition of the MT ligands and ethanolamine, respectively. There are twenty crystallographic sites for the metal cobalt ions, and they display different coordination environment. Nineteen Co^{II} ions (Co1-Co13 and Co15-Co20) display the distorted six-coordinated octahedral geometry, which can be classified as five kinds of coordination environments, and the remaining Co^{II} ion exhibits five-coordinated configuration. In the six-coordinated Co^{II} ions, twelve Co^{II} ions (Co1-Co10, Co13 and Co18) possess the same coordination environment, and each Co^{II} ion is completed with four bridged oxygen atoms, one oxygen atom from $[SO_4]^{2-}$ core and one nitrogen atom from 1,3,4-thiadiazole of MT ligand, which manufacture a classical α-Keggin-type skeleton (Fig. 1b and Fig. S1a). To the best of our knowledge, the report on the construction of α-Keggin structure based on the later transition metals and the organic ligands is rare so far.[15,16b,18d]

The other six-coordinated Co^{II} ions present diverse coordination environments (Fig. S1c). Both Co11 and Co12 are surrounded by three nitrogen atoms from 1,3,4-thiadiazole groups of three separate MT ligands and three bridged oxygen atoms. Both Co15 and Co17 are encircled by two nitrogen atoms from 1,3,4-thiadiazole groups of two separate MT ligands, one sulfur atom from mercapto group of one MT ligand and three bridged oxygen atoms. These four Co^{II} ions (Co11, Co12, Co15 and Co17) are clamped three triad metal units from the α-Keggin skeleton in the form of vertices-sharing. Both Co16 and Co20 are lighted by three sulfur atoms from mercapto groups of three MT ligands and three bridged oxygen atoms. Co19 is furnished by one nitrogen atom of 1,3,4-thiadiazole group, one sulfur atom of mercapto group, three bridged oxygen atoms and one oxygen atom from $[CH_3O]^-$ ion (Fig. S1c). The remaining five-coordinated Co^{II} ion (Co14) displays a distorted {CoO_3NS} square-pyramidal coordination geometry with three bridged oxygen atoms, one nitrogen atom from 1,3,4-thiadiazole group and one sulfur atom from mercapto group (Fig. S1c). All the Co–O, Co–N and Co–S distances are ranging from 1.984(11) Å to 2.495(10) Å, from 2.000(6) Å to 2.330(6) Å and from 2.360(3) Å to 2.564(7) Å, respectively. The above four Co^{II} ions (Co14, Co16, Co19 and Co20) lay in the internal triad metal units from the α-Keggin skeleton in the form of edge-sharing. Eight Co^{II} ions acting as caps all inlay the periphery of α-Keggin polyoxoazocobaltate architecture (Fig.1c). Twenty Co^{II} ions are connected by the bridged oxygen atoms and the organic ligands to generate a homometallic high-nuclearity cluster (Fig. 1a and S1d).

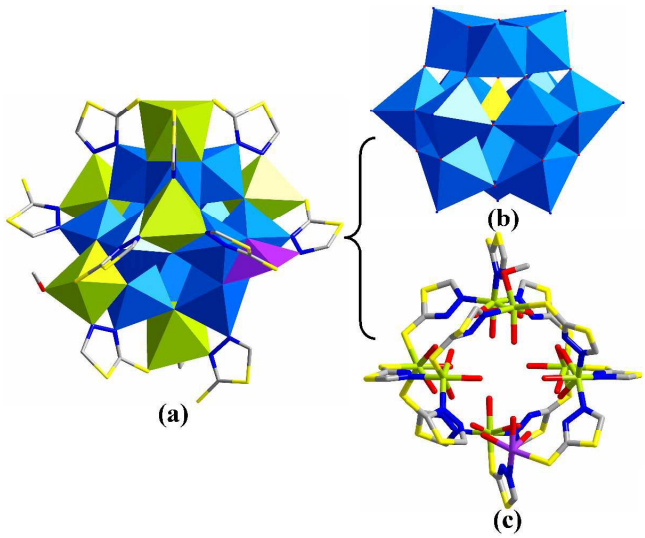

Fig. 1. (a) Polyhedral and stick structure representation of compound **2**; (b) Polyhedral structure representation of the α-Keggin polyoxoazocobaltate core of compound **2**; (c) Stick view of eight peripheral Co^{II} ions of compound **2**. Color legend: olivine, the peripheral octahedral Co; purple, the square-pyramidal Co; azure, the α-Keggin central octahedral Co; gray, C; dark blue, N; red, O; yellow, S. All hydrogen atoms are omitted for clarity.

The twelve organic ligands MT in compound **2** exhibit two kinds of coordination modes (Table. S2). Ten organic MT ligands adopt μ_3-node to coordinate with the metal Co^{II} ions through mercapto group and two nitrogen atoms from 1,3,4-thiadiazole group, respectively. For the other two MT ligands, only the nitrogen atoms from 1,3,4-thiadiazole group bind to the metal Co^{II} ions, which can be viewed as the μ_2-node. It is noted that the mercapto groups are deprotonated, and they are the potential coordination sites, which may further expand the novel structure on the basic of the original high-nuclear homometallic Co^{II} cluster.

Notably, compound **2** not only possesses absorbing structure, but also is a nanoscale cluster in size. The α-Keggin polyoxoazocobaltate ion serving as the centre of cluster is close to the common polyoxometalates (POMs) in dimensions. As shown in Fig. 2a and 2b, the size of polyoxoazocobaltate ion is ca 9.72 Å×11.45 Å, and the size of common POM i.e. SiW_{12} is ca 8.99 Å×10.34 Å.[20] Moreover, the circumjacent semi-enclosed metal-organic cage composed of eight cobalt ions and MT ligands envelops the α-Keggin polyoxoazocobaltate structure, which leads to the formation of the nanoscale homometallic cluster (13.49 Å × 16.16 Å) (Fig. 4a).

Crystal structure of $[Co_{20}(AMT)_{11}(MT)(\mu_3\text{-}OH)_{22}(\mu_3\text{-}O)_2(SO_4)(H_2O)]\cdot EtOH\cdot 4H_2O$ (3)

Compound **3** crystallizing in the triclinic space group *P*-1 reveals a nanosized homometallic Co_{20} cluster including a $[Co_{10}(AMT)_9(MT)(\mu_3\text{-}OH)_{22}(\mu_3\text{-}O)_2]^{16-}$ polyoxoazocobaltate ion (Fig. 3 and Fig. S2c). The generation of both $[SO_4]^{2-}$ and MT ligand may be from decomposition of AMT ligands. Different from compound **2**, the anionic cluster is not the α-Keggin structure but a semi-open $\{Co_{10}\}$ metallic cluster (Fig. S2a). The ten Co^{II} ions are in the form of $2Co^{II}$-$5Co^{II}$-$3Co^{II}$ in the upper, middle and lower layers (Fig. 3b), respectively, in which ten Co^{II} ions all exhibit five-coordinated square pyramidal configuration. Each Co^{II} ion from the upper and middle layers is occupied by one nitrogen atom from 1,3,4-thiadiazole groups of AMT ligand and four bridged oxygen atoms (Fig. S2a). Those three Co^{II} ions adopting η^5 coordination mode from the lower layer coordinate with the different atoms of different ligands. The coordinated environment of Co4 is the same as that of above seven Co^{II} atoms from the upper and middle layers. Co13 is lighted by one sulfur atom from mercapto group of AMT ligand and four bridged oxygen atoms, and Co3 is surrounded by one nitrogen atom from 1,3,4-thiadiazole groups of MT ligand and four bridged oxygen atoms (Fig. S2a). These neighboring five-coordinated Co^{II} ions are in the form of vertices-sharing, resulting in a semi-open $\{Co_{10}\}$ cluster (Fig. 3b).

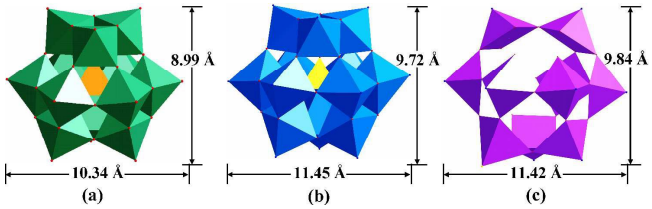

Fig. 2. (a) The traditional α-Keggin POMs (SiW_{12}) based on the early transition metals; (b) The α-Keggin polyoxoazocobaltate core of compound **2**; (c) The semi-open $\{Co_{10}\}$ polyoxoazocobaltate core of compound **3**.

The peripheral Co^{II} ions with η^6 coordination mode are inset in the outer sphere of the $\{Co_{10}\}$ metallic cluster (Fig. 3c). Ten Co^{II} ions display seven kinds of coordination environments with octahedral sphere. Both Co2 and Co9 are environed by one nitrogen atom from 1,3,4-thiadiazole group, four bridged oxygen atoms and one oxygen atom from $[SO_4]^{2-}$ (Fig. S2b). Both Co12 and Co15 are furnished by one nitrogen atom from 1,3,4-thiadiazole group, two sulfur atoms from mercapto groups of two separate AMT ligands and three bridged oxygen atoms (Fig. S2b). Both Co16 and Co17 are lighted by one sulfur atom from mercapto groups, two nitrogen atoms from 1,3,4-thiadiazole groups of two separate AMT ligands and three bridged oxygen atoms (Fig. S2b). These six Co^{II} ions are divided into two groups of edge-sharing triad metal units (Co15-Co2-Co17 and Co16-Co9-Co12), in which Co15, Co2 and Co17 ions arrange breadthwise, inlaying between the upper and middle layers, while Co16, Co9 and Co12 ions arrange lengthwise in the middle layer (Fig. S3).

The remaining four six-coordinated Co^{II} ions are edge-sharing with three vertices-sharing five-coordinated Co^{II} ions, respectively. Co20 is occupied by three sulfur atoms from mercapto groups of two separate AMT ligands and three bridged oxygen atoms, locating between the upper and middle layers. Co19 is bonded by three nitrogen atoms from 1,3,4-thiadiazole group and three bridged oxygen atoms, and Co14 attaches to two nitrogen atoms from 1,3,4-thiadiazole groups of one AMT ligand and one MT ligand, one sulfur atom from mercapto group of one AMT ligand, and three bridged oxygen atoms. Both of them locate inside between the middle and lower layers. Co18 is coordinated with one nitrogen atom from 1,3,4-thiadiazole group of one AMT ligand, one sulfur atom from mercapto group of MT

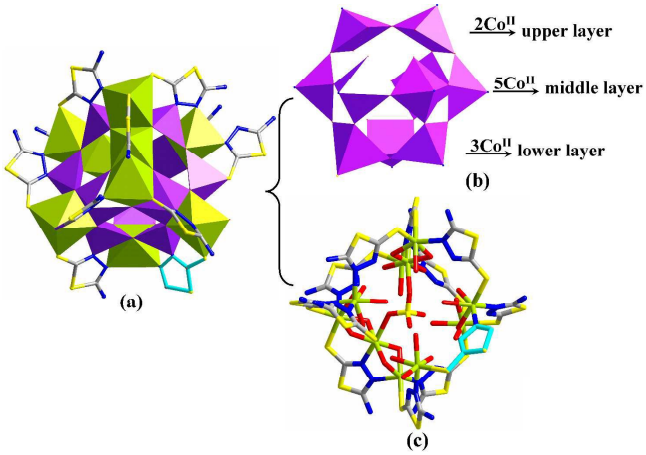

Fig. 3. (a) Polyhedral and stick structure representation of compound **3**; (b) Polyhedral structure representation of the semi-open $\{Co_{10}\}$polyoxoazocobaltate core of compound **3**; (c) Stick view of ten peripheral Co^{II} ions of compound **3**. Color legend: olivine, the peripheral octahedral Co; purple, the square-pyramidal Co; gray, C; dark blue, N; red, O; yellow, S. All hydrogen atoms are omitted for clarity.

ligand and four bridged oxygen atoms, locates in vertices-sharing triad metal units from the lower layer (Fig. S2b and S3). All the Co–O, Co–N and Co–S distances are ranging from 2.012(10) Å to 2.468(11) Å, from 2.044(16) Å to 2.297(13) Å and from 2.485(5) Å to 2.658(5) Å, respectively. The cage consisting of peripheral ten Co^{II} ions is large enough to accommodate the semi-open Co_{10} metallic cluster with the size of 9.84 Å × 11.42 Å (Fig. 2c), forming a homometallic high-nuclearity nanoscale cluster with the size of 14.59 Å × 16.52 Å (Fig. 4b). The sizes of both the central polyoxoazocobaltate ion and the whole nanoscale cluster from compound **3** are larger than that from compound **2**.

For twelve organic ligands, ten AMT ligands and one MT ligand derived from AMT present μ_3-connected coordination pattern, in which three potential coordination sites all join with the metal Co^{II} ions. The other AMT ligand adopts μ_2-connected coordination pattern (one nitrogen atom and one sulfur atom), and the non-coordinated nitrogen atom is in favour of extending dimensionality based on the high-nuclear Co^{II} cluster.

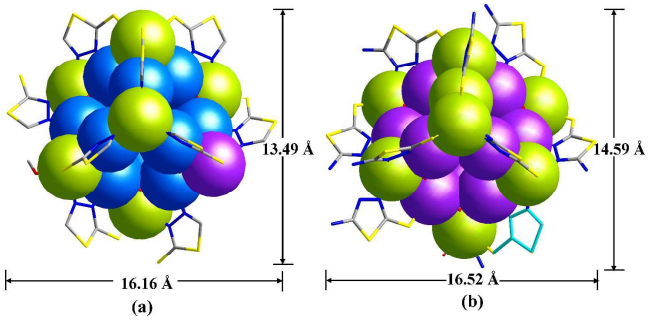

Fig. 4. (a) Space-filling and stick view of $\{Co_{20}\}$ nanocluster of compound **2**. (b) Space-filling and stick view of $\{Co_{20}\}$ nanocluster of compound **3**.

Influence of the Mercapto-based Sulfur Aza-heterocyclic Ligands on the Nanoscale cluster

We selected the different mercapto-based sulfur aza-heterocyclic ligands (MMT, MT and AMT) as the organic ligands to intend to investigate their influences on construction of the homocobaltic high-nuclearity nanoscale clusters. In the three organic ligands, the differences of substituent groups have effect on not only the coordination modes of ligands, but also coordinated numbers of metal ions. The different saturated status from metal ions changes the metal activity sites, which may lead to the differences in properties. As shown in Table. S2, for compound **1**, when the substituent group is methyl ($-CH_3$), MMT ligand only show a kind of μ_3-coordination mode. Each Co^{II} ion locates in the saturated octahedral geometry, resulting in a high symmetric Co_{20} cluster. In compound **2**, there is no substituent group in the sulfur aza-heterocyclic ligand, and MT displays μ_2- and μ_3-coordination mode. Nineteen Co^{II} ions present six-coordinated octahedral configuration, and the remaining peripheral Co^{II} ion lies at square-pyramidal style, leading to the formation of non-symmetric Co_{20} cluster. When the methyl from MMT of compound **1** is replaced by amino from AMT of compound **3**, not only AMT possess two types of coordination modes, but also the new ligand MT is generated by the decomposition of AMT. For the metal cobalt ions, except for the peripheral saturated octahedral sphere, ten unsaturated five-coordinated Co^{II} ions as Co_{10} cluster are in the centre of the whole nanoscale cluster, forming a non-symmetric high-nuclear cluster. From the structural point of view, compared with compound **1**, although compounds **2** and **3** have no high symmetric structure, the non-coordinated atoms from the organic ligands (MT and AMT) have potential coordination capacity, which may be beneficial to enlarge the size of homometallic cluster or yield multi-dimensional architecture based on the nanoscale Co^{II} cluster.

Powder X-ray diffraction

The X-ray powder diffraction (XRPD) patterns of compounds **2**–**3** have been detected at room temperature in order to prove the purity of compounds (Fig. S4). The diffraction patterns from the as-synthesized compounds match the simulated peaks, confirming the phase purities of the samples. The differences of intensity may be attributed to the preferred orientation of the crystals.

Thermal stability analysis

Thermal behaviors of compounds **2**–**3** were explored by thermogravimetric analyses (TGA) in the temperature range of 30–800 °C under nitrogen atmosphere. As shown in Fig. S5, the TGA curve of compound **2** includes two steps of weight losses. The first weight loss of 2.78% at 30–95 °C range may be attributed to the the loss of ethanol (calcd 2.86%). The second weight loss of 47.50% occurs from 95 °C to 750 °C, which may be close to decomposition of host structure (calcd 50.47%). The remaining weight (50.02%) correlates with the CoO (calcd 46.67%). For compound **3**, the first weight loss (3.59%) may be due to the loss of ethanol and lattice water molecules (calcd 3.48%), The second wieght loss (49.37%) starts at 143 °C and finishes by 750 °C, corresponding to the loss of coordinated water molecules and the collapse of host structure (calcd 52.29%). The remaining residues may be ended with CoO formation.

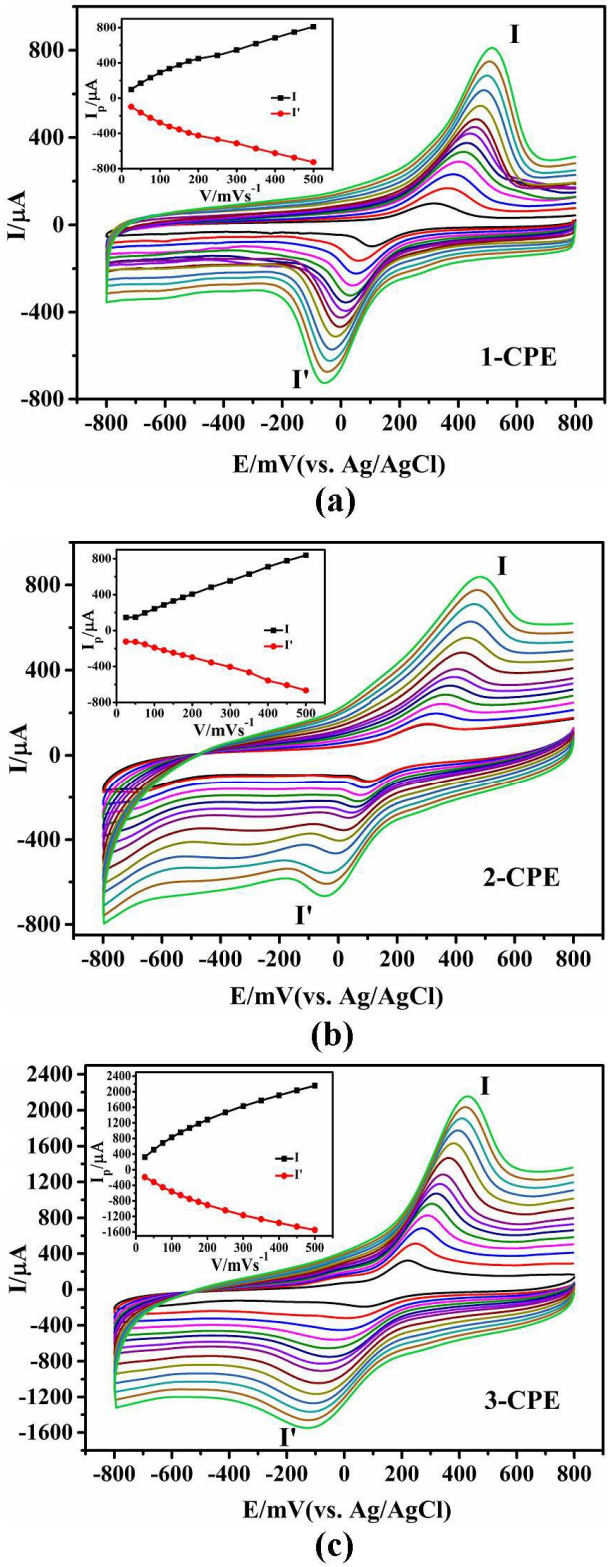

Fig. 5. Cyclic voltammograms of the **1**–, **2**– and **3**–CPE in 0.01 M H_2SO_4 + 0.5 M Na_2SO_4 aqueous solution at different scan rates (from inner to outer: 25, 50, 75, 100, 125, 150, 175, 200, 250, 300, 350, 400, 450, 500 mVs^{-1}). The inset shows the plots of the anodic and cathodic peak currents against scan rates.

Electrochemical behaviors of 1–3–CPEs

In some important properties of cobalt clusters, the reversible redox process in the field of electrochemistry has great attraction.[21] In order to investigate redox properties of the homometallic nanoscale cobalt clusters, compounds **1**–**3** bulk-modified carbon paste electrodes (**1**–, **2**– and **3**–CPE) were used as the working electrodes due to their insolubility in water and the common organic solvent. The cyclic voltammograms of **1**– ~ **3**–CPE were measured in 0.01 M H_2SO_4 + 0.5 M Na_2SO_4 aqueous solution with the diverse scan rates in the potential range of 800 to –800 mV. As shown in Fig. S6, there is no redox peak at the bare CPE, while a pair of redox peaks appears at the modified **1**– ~ **3**–CPE, respectively, which may be ascribed to the redox of Co^{III}/Co^{II}.[22] The mean peak potentials $E_{1/2} = (E_{pa} + E_{pc})/2$ are approximately 221 mV for **1**–CPE, 215 mV for **2**–CPE and 126 mV for **3**–CPE at the scan rate of 100 mVs^{-1}, respectively. Influences of scan rates on the electrochemical behaviour for **1**– ~ **3**–CPE are shown in Fig. 5, the redox peak potentials shifted gradually with the increasing scan rates from 25 to 500 mV s^{-1}: the cathodic peak potentials shifted towards negative direction and the relevant anodic peak potentials shifted towards positive direction. The inset of Fig. 5 displays the plots of peak currents versus scan rates, and both anodic and the cathodic peak currents are proportional to the scan rates, which indicates that the redox processes of **1**– ~ **3**–CPE are surface-controlled.

Photocatalytic activity

Organic dyes as a kind of harmful contaminant are difficult to be degraded by means of conventional treatments on account of their high solubility in water. Photocatalytic degradation is an effective method in decomposing organic dyes, and the organic dyes is gradually decomposed into nonpolluting small organic acids and CO_2 in this catalytic process. The insoluble homometallic nanoscale clusters can be regarded as the good candidates for degrading the organic compounds. To research the photocatalytic activities of Co^{II} multinuclear clusters further, methyl orange (MO), methylene blue (MB) and rhodamine B (RhB), as models of dye pollutant, are selected for evaluating the photocatalytic effectiveness in the course of purifying wastewater. In the course of the photocatalytic degradation for compounds **1**–**3**, the visible light induces sulfur aza-heterocyclic ligands to generate nitrogen-Co^{II} charge transfer, which promote electrons from the highest occupied molecular orbital (HOMO) to the lowest unoccupied molecular orbital (LUMO). The HOMO strongly requires one electron to go back to its stable state, so the electron is caught from water molecules, which is oxygenated to produce the ·OH radicals. Then the organic dyes may be disintegrated by ·OH active species effectively, which finish the photocatalytic process.[23]

The photocatalytic experiments were performed in a typical process, 30 mg catalysts were added into 200 ML aqueous solution of three kinds of organic dyes with the concentration of 10.0 mg /L, and the mixture was magnetically stirred in the dark for 30 min in order to reach an adsorption/desorption equilibrium. Afterward, the solution was exposed to visible light irradiation from an xenon lamp, in the process of which the solution was stirred continuously in the center of the reactive apparatus. 3 mL of sample solution was taken from the vessel every 20 min, and they were subsequently analyzed by visible spectroscopy. The

comparative experiment of organic dyes degradation was also carried out under the same conditions without any catalyst.

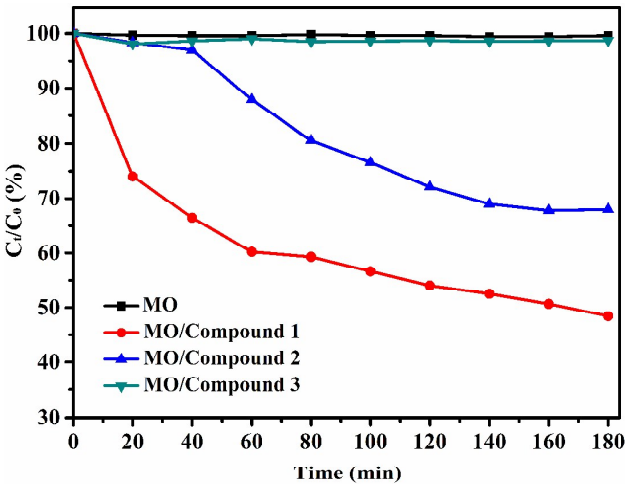

Fig. 6. Photocatalytic decomposition rates of MO solution under visible-light irradiation with the use of compounds **1**–**3** and the control experiment without any catalyst in the same conditions.

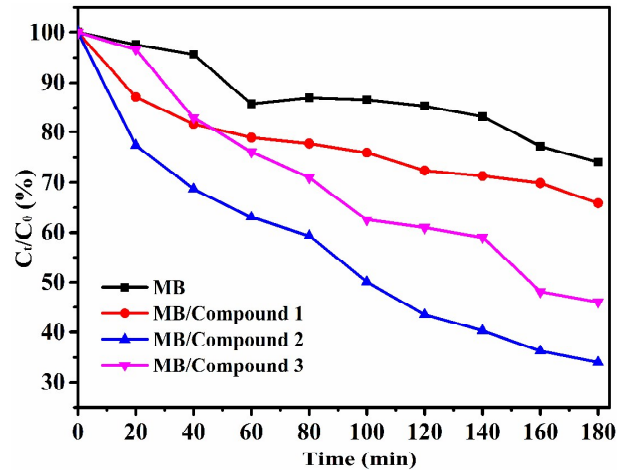

Fig. 7. Photocatalytic decomposition rates of MB solution under visible-light irradiation with the use of compounds **1**–**3** and the control experiment without any catalyst in the same conditions.

As illustrated in Fig. S7a, no change in the degradation of MO under the visible-light could be observed without photocatalysts. The characteristic absorbance of MO decreased with longer illumination time in the presence of compounds **1** and **2**, while compound **3** has no change in the degradation of MO (Fig. S7f–h). As shown in Fig. 6, the concentrations of MO (C) versus irradiation times (t) of compounds **1**–**3** are plotted. The degradations increases from about 0.4% (without any catalyst) to 51.6% for **1**, 32.1% for **2** and 1.3% for **3** after 180 min irradiation. The above results show that the photocatalytic activities of compounds **1**–**2** for the degradation of MO decrease in turn. While the degradation of only 1.3% from compound **3** may be owing to the experimental error, therefore, compound **3** should be no degradation effect. Control experiments of the title reactants have also been examined. The $Co(NO_3)_2{\cdot}6H_2O$, MMT, MT and AMT ligands were added to the MO solution with visible light irradiation, respectively. However, MMT, MT and AMT ligands have no photocatalytic behaviors (Fig. 6, Fig. S7c–e and Fig. S8), and $Co(NO_3)_2{\cdot}6H_2O$ exhibits the weak photocatalytic activity (Fig. 6, Fig. S7b and Fig. S8). The above phenomena indicate that the Co^{II} multinuclear clusters compounds **1**–**2** formed by the reactants $Co(NO_3)_2{\cdot}6H_2O$ and the organic ligands may display the photocatalytic activities for the degradation of MO.

The degradation of dye MB is different from that of MO. The absorption peaks of MB reduced obviously for compounds **2**–**3** with increasing reaction time, while compound **1** has the weak change (Fig. 7, Fig. S9f–h and S10). Fig. 7 exhibits the concentrations of MB (C) versus irradiation times (t) of compounds **1**–**3**. The photocatalytic activities increase from 25.2% (without any catalyst) to 34.1% for **1**, 66.0% for **2** and 54.6% for **3**. Control experiments of the title reactants ($Co(NO_3)_2{\cdot}6H_2O$, MMT, MT and AMT ligands) have been examined, which shows that $Co(NO_3)_2{\cdot}6H_2O$ and MT ligand display the weak photocatalytic activity, and the other reactants have no obvious change (Fig. S9b–e). Compared with MB without catalysts, the title compounds all exhibit the photocatalytic activities for the degradation of MB. However, compared with reactant $Co(NO_3)_2{\cdot}6H_2O$, the ability of degradation for compound **1** is weaker. The results illustrate that compounds **2**–**3** have the good effect of degradation relative to compound **1** and the other reactants.

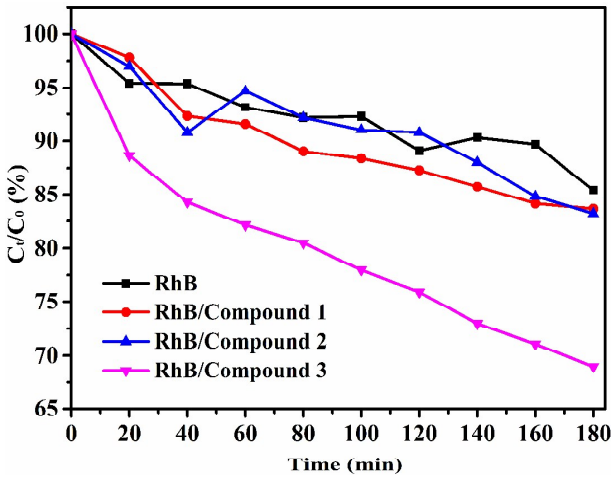

Fig. 8. Photocatalytic decomposition rates of RhB solution under visible-light irradiation with the use of compounds **1**–**3** and the control experiment without any catalyst in the same conditions.

When RhB was chosen as the third model of organic dye, compound **3** displays photocatalytic behavior, however, there is no obvious photocatalytic activity for compounds **1**–**2** (Fig. 8, Fig. S11f–h and S12). In Fig. 8, it shows that the photocatalytic activities increase from 14.6% (without any catalyst) to 16.3% for **1**, 16.8% for **2**, and 31.0% for **3** after 180 min irradiation. The degradation effect of compounds **1**–**2** is close to that of RhB (without any catalyst), which may be due to experimental error, so compounds **1**–**2** should be no photocatalytic activity. The reactants ($Co(NO_3)_2{\cdot}6H_2O$, MMT, MT and AMT ligands) also have been examined in the RhB solution through the visible light irradiation (Fig. S11b–e), and the result displays that the weak photocatalytic activity of metal $Co(NO_3)_2{\cdot}6H_2O$ is close to that of compound **3** (Fig. S12). Compared with RhB without catalysts, compound **3** is active under visible light irradiation. The

photostability of compounds with photocatalytic activities was detected through XRPD after the photocatalytic reactions. The XRPD patterns are identical with those of the simulated compounds, implying that they have the good stability (Fig. S4).

The photocatalytic activities of the title compounds toward degradation of three kinds of organic dyes have been studied. For the degradation of the same organic dye, three multinuclear clusters **1**–**3** show different photocatalytic selectivity, which may be ascribed to charge transfer between the organic ligands and Co center.[24] From the perspective of structure, the results may be due to the differences from coordination environments of the metal Co^{II} ions, the selection of different organic ligands and the final diversities of conjugation and structures of high-nuclearity clusters. It is noted that in the field of coordination compounds, some reported photocatalysts are metal-organic networks or polyoxometalate-based hybrids.[7c,25] However, the research of photocatalysis based on the metal-organic multinuclear nanoclusters has not reported yet so far.

Conclusions

In summary, on the basis of compound **1**, two novel nanoscale high-nuclearity cobalt clusters derived from mercapto-based sulfur aza-heterocyclic ligands have been obtained successfully. Compound **2** is made up of Keggin-type Co_{12} cluster and eight capped Co^{II} ions, which is rare in the cluster-compounds. Compound **3** displays that the inner semi-open Co_{10} polyoxoazocobaltate cluster is encapsulated outer Co_{10} cage. The introduction of the different substituent groups has an effect on coordinated modes of the organic ligands and coordinated status of metal ions. The different metal saturated status may lead to distinctions of metal activity sites, which may have excellent properties in the field of application. The electrochemical behaviors reveal that the title compounds have the potential applications in the electrochemical field. In photocatalytic properties, compounds **1**–**3** possess the photocatalytic selectivity for degradation of some organic dyes, which may be a kind of good photoactive materials.

Acknowledgements

This work was supported by the Program for National Nature Science Foundation of China (nos. 21271024 and 20971014) and Beijing Natural Science (no. 2112037).

Notes and references

1 (a) D. Ravelli, D. Dondi, M. Fagnoni, A. Albini, *Chem. Soc. Rev.*, 2009, **38**, 1999; (b) A. Kudo, Y. Miseki, *Chem. Soc. Rev.*, 2009, **38**, 253; (c) A. Hagfeldt, G. Boschloo, L. Sun, L. Kloo, H. Pettersson, *Chem. Rev.*, 2010, **110**, 6595; (d) A. Sartorel, M. Bonchio, S. Campagnab, F. Scandola, *Chem. Soc. Rev.*, 2013, **42**, 2262; (e) S. Sarina, H. Zhu, Z. Zheng, S. Bottle, J. Chang, X. Ke, J. C. Zhao, Y. Huang, A. Sutrisno, M. Willans, G. Li, *Chem. Sci.*, 2012, **3**, 2138.

2 (a) M. Liang, J. Chen, *Chem. Soc. Rev.*, 2013, **42**, 3453; (b) I. D. Rattee, *Chem. Soc. Rev.*, 1972, **1**, 145; (c) A. Hagfeldt, G. Boschloo, L. C. Sun, L. Kloo, H. Pettersson, *Chem. Rev.*, 2010, **110**, 6595.

3 (a) M. T. Uddin, M. A. Islam, S. Mahmud, M. Rukanuzzaman, *J. Hazard. Mater.*, 2009, **164**, 53; (b) C. A. Martınez-Huitle, E. Brillas, *Appl. Catal., B.*, 2009, **87**, 105.

4 (a) P. P. Zhang, J. Peng, H. J. Pang, J. Q. Sha, M. Zhu, D. D. Wang, M. G. Liu, Z. M. Su, *Cryst. Growth Des.*, 2011, **11**, 2736; (b) C. Tian, Q. Zhang, A. Wu, M. Jiang, Z. Liang, B. Jiang, H. Fu, *Chem. Commun.*, 2012, **48**, 2858; (c) J. M. R. Narayanam, C. R. J. Stephenson, *Chem. Soc. Rev.*, 2011, **40**, 102.

5 (a) A. Fujishima, X. Zhang, D. Tryk, A. *Surf. Sci. Rep.*, 2008, **63**, 515; (b) A. Kar, Y. R. Smith, V. Subramanian, *Environ. Sci. Technol.*, 2009, **43**, 3260; (c) H. X. Li, X. Y. Zhang, Y. N. Huo, J. Zhu, *Environ. Sci. Technol.*, 2007, **41**, 4410.

6 (a) X. L. Wang, J. Luan, F. F. Sui, H. Y. Lin, G. C. Liu, C. Xu, *Cryst. Growth Des.*, 2013, **13**, 3561; (b) Z. L. Liao, G. D. Li, M. H. Bi, J. S. Chen, *Inorg. Chem.*, 2008, **47**, 11.

7 (a) Y. Q. Chen, S. J. Liu, Y. W. Li, G. R. Li, K. H. He, Y. K. Qu, T. L. Hu, X. H. Bu, *Cryst. Growth Des.*, 2012, **12**, 5426; (b) L. L. Wen, J. B. Zhao, K. L. Lv, Y. H. Wu, K. J. Deng, X. K. Leng, D. F. Li, *Cryst. Growth Des.*, 2012, **12**, 1603; (c) J. Guo, J. Yang, Y. Y. Liu, J. F. Ma, *CrystEngComm*, 2012, **14**, 6609.

8 (a) X. L. Wang, J. J. Huang, L. L. Liu, G. C. Liu, H. Y. Lin, J. W. Zhang, N. L. Chen, Y. Qu, *CrystEngComm*, 2013, **15**, 1960; (b) X. L. Wang, F. F. Sui, H. Y. Lin, J. W. Zhang, G. C. Liu, *Cryst. Growth Des.*, 2014, **14**, 3438; (c) A. K. Paul, R. Karthik, S. Natarajan, *Cryst. Growth Des.*, 2011, **11**, 5741.

9 (a) A. Douvali, G. S. Papaefstathiou, M. P. Gullo, A. Barbieri, A. C. Tsipis, C. D. Malliakas, M. G. Kanatzidis, I. Papadas, G. S. Armatas, A. G. Hatzidimitriou, T. Lazarides, M. J. Manos, *Inorg. Chem.*, 2015, **54**, 5813; (b) J. Y. Yang, L. Zhou, J. G. Cheng, Z. W. Hu, C. Y. Kuo, C. W. Pao, L. Y. Jang, J. F. Lee, J. H. Dai, S. J. Zhang, S. M. Feng, P. P. Kong, Z. Yuan, J. Yuan, Y. Uwatoko, T. Liu, C. Q. Jin, Y. W. Long, *Inorg. Chem.*, 2015, **54**, 6433; (c) V. N. Vukotic, C. A. O'Keefe, K. L. Zhu, K. J. Harris, C. To, R. W. Schurko, S. J. Loeb, *J. Am. Chem. Soc.*, 2015, **137**, 9643; (d) Y. Y. Liu, A. J. Howarth, J. T. Hupp, O. K. Farha, *Angew. Chem.*, 2015, **127**, 9129.

10 (a) J. B. Pyser, D. Aulakh, X. Zhang, A. A. Yakovenko, K. R. Dunbar, M. Wriedt, *J. Am. Chem. Soc.*, 2015, **137**, 9254; (b) Y. F. Bi, S. T. Wang, M. Liu, S. C. Du, W. P. Liao, *Chem. Commun.*, 2013, **49**, 6785; (c) Z. L. Chen, M. M. Jia, Z. Zhang, F. P. Liang, *Cryst. Growth Des.*, 2010, **10**, 11; (d) J. Li, Y. Guo, H. R. Fu, J. Zhang, R. B. Huang, L. S. Zheng, J. Tao, *Chem. Commun.*, 2014, **50**, 9161; (e) C. B. Tian, Z. J. Lin, S. W. Du, *Cryst. Growth Des.*, 2013, **13**, 3746; (f) P. S. Perlepe, A. A. Athanasopoulou, K. I. Alexopoulou, C. P. Raptopoulou, V. Psycharis, A. Escuer, S. P. Perlepes, T. C. Stamatatos, *Dalton Trans.*, 2014, **43**, 16605; (g) T. L. Hu, J. R. Li, C. S. Liu, X. S. Shi, J. N. Zhou, X. H. Bu, J. Ribas, Inorg. Chem., 2006, **45**, 162.

11 (a) K. Zhou, C. Qin, X. L. Wang, L. K. Yan, K. Z. Shao, Z. M. Su, *CrystEngComm*, 2014, **16**, 10376; (b) K. Zhou, C. Qin, X. L. Wang, K. Z. Shao, L. K. Yan, Z. M. Su, *CrystEngComm*, 2014, **16**, 7860; (c) K. Zhou, C. Qin, X. L. Wang, K. Z. Shao, L. K. Yan, Z. M. Su, *Dalton Trans.*, 2014, **43**, 10695; (d) Y. Q. Hu, M. H. Zeng, K. Zhang, S. Hu, F. F. Zhou, M. Kurmoo, *J. Am. Chem. Soc.*, 2013, **135**, 7901; (e) Y. Y. Cao, Y. M. Chen, L. Li, D. D. Gao, W. Liu, H. L. Hu, W. Li, Y. H. Li, *Dalton Trans.*, 2013, **42**, 10912; (f) S. S. Mondal, A. Bhunia, A. Kelling, U. Schilde, C. Janiak, H. J. Holdt, *Chem. Commun.*, 2014, **50**, 5441; (g) G. N. Newton, G. J. T. Cooper, P. Kogerler, D. L. Long, L. Cronin, *J. Am. Chem. Soc.*, 2008, **130**, 790.

12 S. K. Langley, R. A. Stott, N. F. Chilton, B. Moubaraki, K. S. Murray, *Chem. Commun.*, 2011, **47**, 6281.

13 (a) K. Zhou, Y. Geng, L. K. Yan, X. L. Wang, X. C. Liu, G. G. Shan, K. Z. Shao, Z. M. Su, Y. N. Yu, *Chem. Commun.*, 2014, **50**, 11934; (b) K. Zhou, C. Qin, H. B. Li, L. K. Yan, X. L. Wang, G. G. Shan, Z. M. Su, C. Xu, X. L. Wang, *Chem. Commun.*, 2012, **48**, 5844.

14 (a) G. Li, Z. Lei, Q. M. Wang, *J. Am. Chem. Soc.*, 2010, **132**, 17678; (b) J. Qiao, K. Shi, Q. M. Wang, *Angew. Chem. Int. Ed.*, 2010, **49**, 1765.

15 (a) L. J. Dong, R. D. Huang, Y. G. Wei, W. Chu, *Inorg. Chem.*, 2009, **48**, 7528; (b) L. J. Dong, X. F. Li, J. Cao, W. Chu, R. D. Huang, *Dalton Trans.*, 2013, **42**, 1342.

16 (a) J. Esteban, L. Alcazar, M. Torres-Molina, M. Monfort, M. Font-Bardia, A. Escuer, *Inorg. Chem.*, 2012, **51**, 5503; (b) A. Bino, M. Ardon, D. Lee, B. Spingler, S. J. Lippard, *J. Am. Chem. Soc.*, 2002, **124**, 4578; (c) K. Z. Su, F. L. Jiang, J. J. Qian, J. D. Pang, S. A. AL-Thabaiti, S. M. Bawaked, M. Mokhtar, Q. H. Chen, M. C. Hong, *Cryst. Growth Des.*, 2014, **14**, 5865.

17 (a) M. Lamouchi, E. Jeanneau, G. Novitchi, D. Luneau, A. Brioude, C. Desroches, *Inorg. Chem.*, 2014, **53**, 63; (b) K. Zhou, C. Qin, L. K. Yan, F. M. Wang, Z. M. Su, *RSC Adv.*, 2014, **4**, 60451.

18 (a) M. L. Tong, M. Monfort, J. M. C. Juan, X. M. Chen, X. H. Bu, M. Ohbad, S. Kitagawa, *Chem. Commun.*, 2005, 233; (b) K. Zhou, X. L. Wang, C. Qin, H. N. Wang, G. S. Yang, Y. Q. Jiao, P. Huang, K. Z. Shao, Z. M. Su, *Dalton Trans.*, 2013, **42**, 1352; (c) A. J. Zhou, J. D. Leng, J. S. Hua, M. L. Tong, *Dalton Trans.*, 2013, **42**, 9428; (d) O. Sadeghi, L. N. Zakharov, M. Nyman, *Science*, 2015, **347**, 1359.

19 (a) G. M. Sheldrick, *Acta Crystallogr. A.*, 2008, **64**, 112; (b) PLATON program: A. L. Spek, *Acta Crystallogr., Sect. A: Found. Crystallogr.*, 1990, **46**, 194.

20 A. X. Tian, J. Ying, J. Peng, J. Q. Sha, H. J. Pang, P. P. Zhang, Y. Chen, M. Zhu, Z. M. Su, *Inorg. Chem.*, 2009, **48**, 100.

21 (a) W. Li, S. Z. Zhan, J. G. Wang, W. Y. Yan, Y. F. Deng, *Inorg. Chem. Commun.*, 2008, **11**, 681; (b) K. Winkler, M. E. Plonska, A. Basa, M. Lach, A. L. Balch, *Electroanalysis*, 2003, **15**, 55.

22 T. V. Mitkina, N. F. Zakharchuk, D. Y. Naumov, O. A. Gerasko, D. Fenske, V. P. Fedin, *Inorg. Chem.*, 2008, **47**, 6748.

23 (a) H. X. Yang, T. F. Liu, M. N. Cao, H. F. Li, S. Y. Gao, R. Cao, *Chem. Commun.*, 2010, **46**, 2429; (b) J. X. Meng, Y. Lu, Y. G. Li, H. Fu, E. B. Wang, *CrystEngComm*, 2011, **13**, 2479; (c) J. Guo, J. Yang, Y. Y. Liu, J. F. Ma, *CrystEngComm*, 2012, **14**, 6609.

24 (a) X. L. Wang, N. Li, A. X. Tian, J. Ying, T. J. Li, X. L. Lin, J. Luan, Y. Yang, *Inorg. Chem.*, 2014, **53**, 7118; (b) T. H. Li, S. Y. Gao, F. Li, R. J. Cao, *Colloid Interface Sci.*, 2009, **338**, 500; (c) A. Dolbecq, P. Mialane, B. Keita, L. Nadjo, J. Mater. Chem. 2012, 22, 24509.

25 (a) H. S. Lin, P. A. Maggard, *Inorg. Chem.*, 2008, **47**, 8044; (b) W. Q. Kan, B. Liu, J. Yang, Y. Y. Liu, J. F. Ma, *Cryst. Growth Des.*, 2012, **12**, 2288; (c) A. K. Paul, R. Karthik, S. Natarajan, *Cryst. Growth Des.*, 2011, **11**, 5741.

The Photocatalysis from a Series of Polyoxoazocobaltate High-nuclearity Nanoclusters

Bao Mu, Qing Wang and Rudan Huang*

Key Laboratory of Cluster Science of Ministry of Education, School of Chemistry, Beijing Institute of Technology, Beijing, 100081, P. R. China

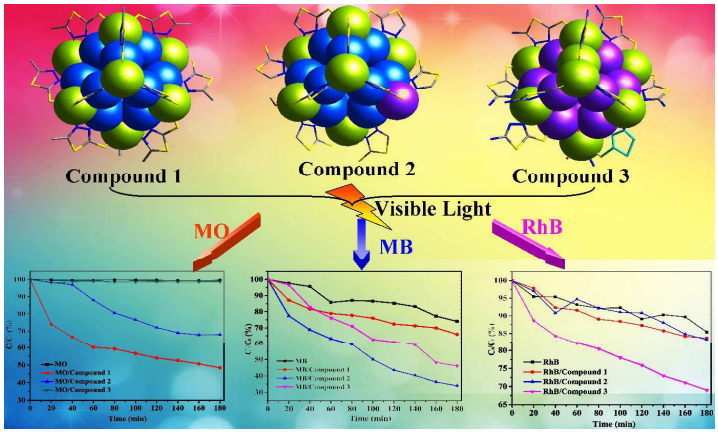

By changing the substituent groups of mercapto-based sulfur aza-heterocyclic ligands, a series of polyoxoazocobaltate high-nuclearity nanoclusters have been synthesized and structurally characterized, and they display photocatalytic activities for degradation of the different organic dyes.

* Corresponding author.

E-mail address: huangrd@bit.edu.cn (R.-D. Huang)